Measurements of the triple-differential cross section for low-energy electron-impact ionization of helium

E. C. Beaty,* K. H. Hesselbacher,† S. P. Hong, and J. H. Moore‡
Joint Institute for Laboratory Astrophysics, National Bureau of Standards and University of Colorado, Boulder, Colorado 80309
(Received 19 July 1977)

The triple-differential cross section for ionization of helium by low-energy electron impact is investigated over the energy and angular variables. Measurements have been made for primary electron energies near 100 eV, ejected electron energies of 5, 10, and 20 eV, and scattering angles 15°, 20°, and 30°. The forward lobe of the triple-differential cross section is found to be approximately cylindrically symmetric.

I. INTRODUCTION

Ionization of atoms by electron impact has been studied for a long time in a great many places. The atom most commonly examined has been helium. The reaction is conventionally written

$$e + \mathrm{He} \rightarrow \mathrm{He}^+ + 2e . \tag{1}$$

The total ionization cross section is obtained by looking for ion production and the double-differential cross section is measured by looking for either one of the two outgoing electrons. Many workers have examined this reaction by looking at both outgoing electrons for cases in which all electron trajectories lie in a plane[1-6] or both outgoing electrons are constrained to a symmetric configuration.[7-14] Here we report observations of both electrons without the above restrictions.

The principle of the measurement is best described by reference to an idealized situation. Suppose a gas of helium atoms of density $N(\vec{r})$ is bombarded by a stream of electrons of energy E_0 and current density $\vec{J}_e(\vec{r})$. All the electrons are assumed to be moving in the same direction and $N(\vec{r})$ and $\vec{J}_e(\vec{r})$ are assumed relatively constant over some small volume $\delta\vec{r}$. Therefore, only the magnitude of the current density $J_e(\vec{r})$ needs to be considered. Reaction (1) will cause the appearance of positive ions and free electrons with energy less than E_0. Arrange one electron analyzer detector to detect those electrons moving in direction $\vec{k}_a$ within solid angle $\delta\Omega_a$, and with energy E_a within some tolerance δE_a. Arrange another electron detector with similar characteristics which are distinguished by the subscript b. If the current of primary electrons is small enough, it is possible to select with little ambiguity those occasions when the electrons in the two detectors come from the same ionization event. The main interest here is in these "coincident" events. If the outgoing electrons have energies E_a and E_b, the excitation energy of the ion is $E_i = E_0 - E_a - E_b - \mathrm{IP}$, where IP is the ionization potential of the target gas. In this measurement, we are only interested in the case where the ion is in its ground state ($E_i = 0$). Since E_b is a function of E_a for a known incident electron energy and target gas, E_b is not an independent variable. The rate of coincident events in $\delta\vec{r}$ can be expressed

$$\frac{d^3\sigma}{dE_a d\Omega_a d\Omega_b} N(\vec{r}) J_e(\vec{r}) \delta\vec{r}\, \delta E_a \delta\Omega_a \delta\Omega_b , \tag{2}$$

where the quantity $d^3\sigma/dE_a\, d\Omega_a\, d\Omega_b$ is conventionally called the triple-differential cross section. As defined above, the triple-differential cross section provides a full description of the kinematics of the two outgoing electrons for a particular energy state of the ion (ignoring spin). The principle of conservation of momentum allows the computation of the momentum of the positive ion. Thus, for this case the triple-differential cross section may be referred to as the complete-differential ionization cross section.

Specification of the final state of reaction (1) requires nine simple kinematic variables for each state of the ion. For a given state of the ion, four of these are related to the others by the equations expressing conservation of energy and momentum. In addition the initial system is cylindrically symmetric so one other variable is cyclic. The result is that the complete-differential ionization cross section for each ion state is a function of E_0 and four final-state variables. The final-state variables chosen in this report are the energy of one of the electrons E_a and three angles specifying the direction of motion of the electrons. The full five-dimensional space is so large that there is no prospect for exploring all of it. Prior work[1-15] provides information on the complete-differential ionization cross section for selected domains in this five-dimensional space. The first measurements were reported by Ehrhardt *et al.*[2,3] who gave angular-distribution data with the constraint that the three electron trajectories are in a plane. Data were reported for low incident energies and several values of the other variables. Hood *et al.*[7,8] have reported data at high incident

energies with other variables selected to insure the validity of a particular quantum-mechanical approximation. The object was to deduce the momentum-space wave function of the target. In a previous paper[15] we have reported measurements of angular distributions for cases selected to facilitate comparison with the Born approximation. In this paper we report further measurements selected to best describe some characteristics of the complete-differential cross section.

II. EXPERIMENTAL APPARATUS

The equipment and operating procedure were set up to approximate the idealized measurement described above. Angular distributions were explored by physically moving some of the components. The relative positions are important for interpreting the data, and different parts of the data are best described using different coordinate systems. As a first step in describing the apparatus we define a coordinate system suitable for specification of the relative positions of the components. The helium gas is in the form of an atomic beam which is cylindrically symmetric and approximately vertical. The axis of symmetry is an important reference line which we label by the unit vector $\vec{z}$. The electron gun and the two electron analyzer detectors also have well-defined mechanical axes which we label with unit vectors $\vec{k}_0$, $\vec{k}_a$, and $\vec{k}_b$, respectively.

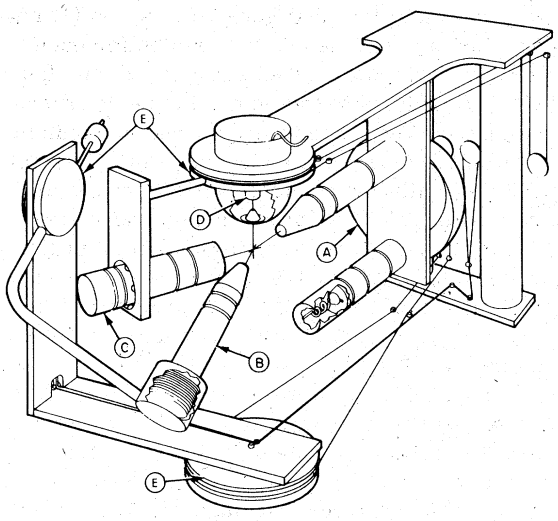

FIG. 1. Electron-impact spectrometer. *A* is the scattered electron analyzer including a hemispherical electrostatic deflector, electrostatic lens systems, and a channel electron multiplier. *B* is the time-of-flight analyzer, *C* is the electron gun, and *D* is the gas jet. *E* indicates the bearings for rotating the gun around the gas beam on one plane and the time-of-flight analyzer around the scattering center in three dimensions.

$\vec{k}_a$ is fixed relative to the vacuum system and is orthogonal to $\vec{z}$. $\vec{k}_0$ can be rotated about an axis coincident with $\vec{z}$ and is always orthogonal to $\vec{z}$. $\vec{k}_0$, $\vec{z}$, and $\vec{k}_a$ all intersect at a point which we call the "scattering center." The plane containing $\vec{k}_0$ and $\vec{k}_a$ is called the "scattering plane." $\vec{k}_b$ can be rotated about either of two axes both of which go through the scattering center such that $\vec{k}_b$ always passes through the scattering center. We define the scattering angle θ_a by the equation $\vec{k}_a \cdot \vec{k}_0 = \cos\theta_a$. Define one further line $\vec{k}_b'$ which is the projection of $\vec{k}_b$ on the scattering plane. The angles chosen to specify $\vec{k}_b$, θ_b, and ϕ_b are such that $\vec{k}_0 \cdot \vec{k}_b' = \cos\theta_b$ and $\vec{k}_b \cdot \vec{k}_b' = \cos\phi_b$.

The apparatus is illustrated in Fig. 1. The electron gun was designed to direct a small pencil of electrons with selected energy E_0 through the scattering center. The source of electrons was a directly heated tungsten filament with no special energy selection. An electrostatic lens was used to produce a well-defined electron beam at the scattering center. Tests showed that the beam diameter at the scattering center was about 1.0 mm and that the beam divergence was about 0.005 rad. The energy width of the beam was measured to be about 0.3 eV and the current was typically of the order of 10^{-8} A.

The helium-gas beam was formed by a small gas jet (a multichannel array with a total diameter of about 1 mm) with a skimmer aperture of 4 mm diameter located 4 cm away. The region between the multichannel array and the skimmer was isolated from the main portion of the vacuum system and evacuated by a separate pump. The distance between the scattering center and the skimmer is 2.5 cm. Tests indicated that in the scattering plane the radial distribution of gas density was approximately Gaussian with the half-intensity point about 3.5 mm from the scattering center. The gas pressure in the interaction region was one order of magnitude greater than the background pressure which was about 5×10^{-5} torr.

The ionization rate is proportional to $N(\vec{r})J_e(\vec{r})$. Because of the shape of $J_e(\vec{r})$, $N(\vec{r})J_e(\vec{r})$ is zero except near a line which is in the scattering plane. The electron analyzer detectors have detection efficiencies which depend not only on the direction and energy of the electron but the position of the trajectory in space. The electrons of interest here can be considered to originate near the scattering center. It is useful to define functions $G_a(\vec{r},\vec{p})$ and $G_b(\vec{r},\vec{p})$ to be the detection efficiencies of the two analyzer detectors for electrons produced at position $\vec{r}$ with momentum $\vec{p}$.

For convenience of later description, we call the outgoing electron with lower energy the ejected electron and the one with higher energy the scat-

tered electron. The simpler of the two analyzer detectors, the one labeled with the subscript b above, was used to detect the ejected electron. It consists of a three-element lens followed by a drift tube all fabricated of molybdenum. The distances from the scattering center to the entrance pupil, whose diameter is 1.2 cm, and the center of the lens are 2.2 and 6.3 cm, respectively. The length of the field-free tube is about 13.5 cm. The analyzer passed those electrons entering the entrance pupil which were within 2.5° of the direction $\vec{k}_b$. A grid eliminated entirely those electrons with energies below some selected energy.

The analyzer detector identified by the subscript a was used to detect the scattered electrons. In addition to the apertures defining an angular range, a hemispherical deflector with inner and outer radii of 5 and 7.5 cm, respectively, was used to provide energy selection. On the input side the entrance aperture has a diameter of 1.2 cm and is 3 cm away from the scattering center. The limiting apertures were a circular pupil placed at the focal point of the first lens and a rectangular slit after the hemispherical deflector. The characteristics of the selected electron trajectories are best described using the images of the two limiting apertures in the field-free space which includes the scattering center. The image of the pupil was at infinity and the image of the slit for the accepted electron energy T_a was at the scattering center. The image of the slit at the scattering center was somewhat smaller than the entrance aperture to the electron optical system. The result was that for electrons with energy T_a, $G_a(\vec{r},\vec{p})$ in the scattering plane was approximately uniform over a rectangle of width 5 mm, and was zero except for those directions of $\vec{p}$ within 1° of the direction $\vec{k}_a$. For electron energies somewhat higher than T_a the image of the slit was below the scattering plane by enough that $G_a(\vec{r},\vec{p})$ was zero at all positions where $J_e(\vec{r})$ was not equal to zero. Thus, the electron beam performed as one slit of a two-slit spectrometer. The energy width of the spectrometer for this set of measurements was 0.6 eV. Both of the electron analyzers are designed to have a field of view big enough to encompass the entire interaction region.

The magnetic field within a sphere of 20 cm radius about the scattering center was reduced to less than 5 mG by a set of orthogonal Helmholtz coils and magnetic shieldings.

III. EXPERIMENT

The procedure used was standard.[1] However, there were features unique to this experiment. Data were recorded by arranging for the arrival of an electron at detector a to start a timer, and for the arrival of an electron at detector b to stop the timer. In this experiment a time-to-amplitude converter was used. If a stop event did not occur within 200 nsec after a start the timer was reset. A stop event while the timer was not running produced no effect. When a stop event stopped the timer, the time was read digitally and the count incremented in the corresponding channel of a multichannel analyzer. In addition, other counters recorded the total number of start and stop events. These data were accumulated for some time, then recorded on punched paper tape for later analysis. The multichannel analysis was done by a small computer, which, also under program control, sets the angles θ_a, θ_b, ϕ_b. The operating procedure was to submit to the minicomputer a table of angles along with other instructions. The minicomputer then set the angles, assembled a data set, changed the angles to the next table entry, and punched the old data while simultaneously assembling a new set. The table of angles was scanned several times to permit a reproducibility check and to minimize the effects of instrumental drift. The total counting time for a fixed set of angle variables was about 2 h.

From knowledge of the net rate of start and stop events, it is possible to compute the expected number of counts in each channel using the assumption that almost all recorded counts are due to uncorrelated events. The first step in the data analysis was to subtract the background of uncorrelated counts. The resultant time-delay spectrum is approximately an energy spectrum of the electrons in the analyzer detector b. This is so because the analyzer detector a is such that all electrons which pass through take approximately the same time. Thus, the values of E_b and δE_b can be determined by averaging a large number of time-delay spectra. With this average the counts due to coincidence could be clearly distinguished from the random effects.

IV. DATA ANALYSIS

The coincidence count rate I_c can be expressed as follows:

$$I_c = \int \frac{d^3\sigma}{d\Omega_a d\Omega_b dE} J_e(\vec{r}) N(\vec{r}) G_a(\vec{r},\vec{p}) \times G_b(\vec{r},\vec{p})\, d\vec{r}\, d\Omega_a\, d\Omega_b\, dE_a . \quad (3)$$

We have made several assumptions to relate the above expression to the experiment: (i) The triple-differential cross section is a constant within the energy and angular acceptances of both analyzer detectors. (ii) The electron lens systems are designed and operated such that the angular accept-

ances are relatively constant over a wide energy range. (iii) As discussed in Sec. II, since the angular acceptance of analyzer b is large enough to contain the scattering volume $\delta\vec{r}$ at any position, $G_b(\vec{r},\vec{p})$ is treated as a constant. In the following discussion, $G_b(\vec{r},\vec{p})$ is assumed to be 100%. With the above assumptions we are able to rewrite Eq. (3) as follows:

$$I_c = \frac{d^3\sigma}{d\Omega_a d\Omega_b dE}\,\Delta\Omega_a\,\Delta\Omega_b G_b \times \int J_e(\vec{r})N(\vec{r})G_a(\vec{r},\vec{p})\,d\vec{r}\,dE_a . \quad (4)$$

The principal emphasis in the present experiment is to determine how the cross section is distributed over the angle and energy variables. Throughout the experiment the electron current and gas density are maintained constant. For a certain scattering angle θ_a and a set of fixed energy variables, the ratio of any two measurements at different values of θ_b and ϕ_b is

$$\frac{I_c}{I_c'} = \frac{d^3\sigma/d\Omega_a d\Omega_b dE}{d^3\sigma'/d\Omega_a d\Omega_b dE} . \quad (5)$$

Hence the shape of the triple-differential cross section can be determined quite accurately. The uncertainty in the relative data is estimated to be about 10%. The uncertainty may come from the statistical fluctuations in the coincidence rate I_c. Also, the effective interaction volume that analyzer b covers may vary slightly from one position to another. Furthermore, the data-analysis model is not perfect.

Due to the relatively small angular acceptance of analyzer a, as the scattering angle varies, the effective interaction volume in the worst case (the scattering angle being 10° and 90°) can differ by 30%. However, data can be adjusted for the known problems and this systematic error can be reduced to less than 3%. This can be accomplished by normalizing to the known absolute elastic scattering data for a wide range of scattering angles. For the measurements reported here the scattering angle varies, at most, only 15°. From simple geometric considerations, the systematic error introduced is less than 3%. Hence we are able to compare the relative magnitudes of two sets of measurements with the same energy variables and different scattering angles.

The detection efficiency $G_a(\vec{r},\vec{p})$ is strongly energy dependent. Since the voltage ratios on the electron lenses are fixed, the lens characteristics are not expected to vary much for different scattered electron energies. In a first-order approximation[16] $G_a(\vec{r},\vec{p})$ is inversely proportional to scattered electron energy. For all the measurements reported in this work, the energy of the scattered electron is kept the same, $E_a = 70.42$ eV. Therefore, $G_a(\vec{r},\vec{p})$ and ΔE_a remain constant.

Although the emphasis is on the relative shape of the cross section, data are reported on an absolute scale. The integral in Eq. (4) can be determined by observing the intensity of elastically scattered 100-eV electrons at 20°:

$$I_{el} = \int J_e'(\vec{r})N(\vec{r})G_a(\vec{r},\vec{p})\sigma_{el}\,d\vec{r} . \quad (6)$$

The absolute elastic scattering cross section σ_{el} is taken from the experimental results of Kurepa and Vuskovic[17] ($\sigma_{el} = 0.376\times10^{-16}$ cm^2 sr^{-1}). In Eq. (6), I_{el} is the elastic scattering electron current and $J_e'(\vec{r})$ is the incident current density. With the assumptions discussed in this section, the uncertainty of the absolute value of the cross section is estimated to be less than a factor of 2.

There are two major sources of error. One is due to the assumption that the detection efficiency of detector b is 100%. The other is due to the uncertainty in the reported absolute elastic scattering cross section.[17-20] 100% detection efficiency is apparently the upper limit. The experimental absolute elastic scattering cross section of helium reported by Kurepa and Vuskovic is also slightly higher than the average of all the reported values. We chose to use their value so that the uncertainties in both sources of error might cancel each other somewhat.

V. RESULTS

The measured triple-differential cross sections of helium as a function of the angles θ_b and ϕ_b of the ejected electron are presented in the polar diagrams of Figs. 2 and 3. The dots are the experimental results and the solid curves are the lines fitting these data points. The diagrams and the solid curves are the lines fitting these data points. The diagrams on the left-hand side [(a)–(c)] show the in-plane scans where $\phi_b = 0°$. The arrows from the bottom to the center indicate the incident electron direction $\vec{k}_0$, the arrows outgoing from the center define the scattered electron direction $\vec{k}_a$. The momentum-transfer direction is indicated by vector $\vec{K}$. The diagrams on the right-hand side [(d)–(f)] are vertical scans. That is, θ_b has been kept constant and only ϕ_b has been varied. For the vertical scans the angle ϕ_b is restricted mechanically to be less than 18° above the plane. The range of ϕ_b close to $-90°$ was avoided to prevent gas injecting directly into the time-of-flight analyzer. Owing to symmetry, the shapes of the cross section above and below the scattering plane are expected to be mirror images, and data taken above

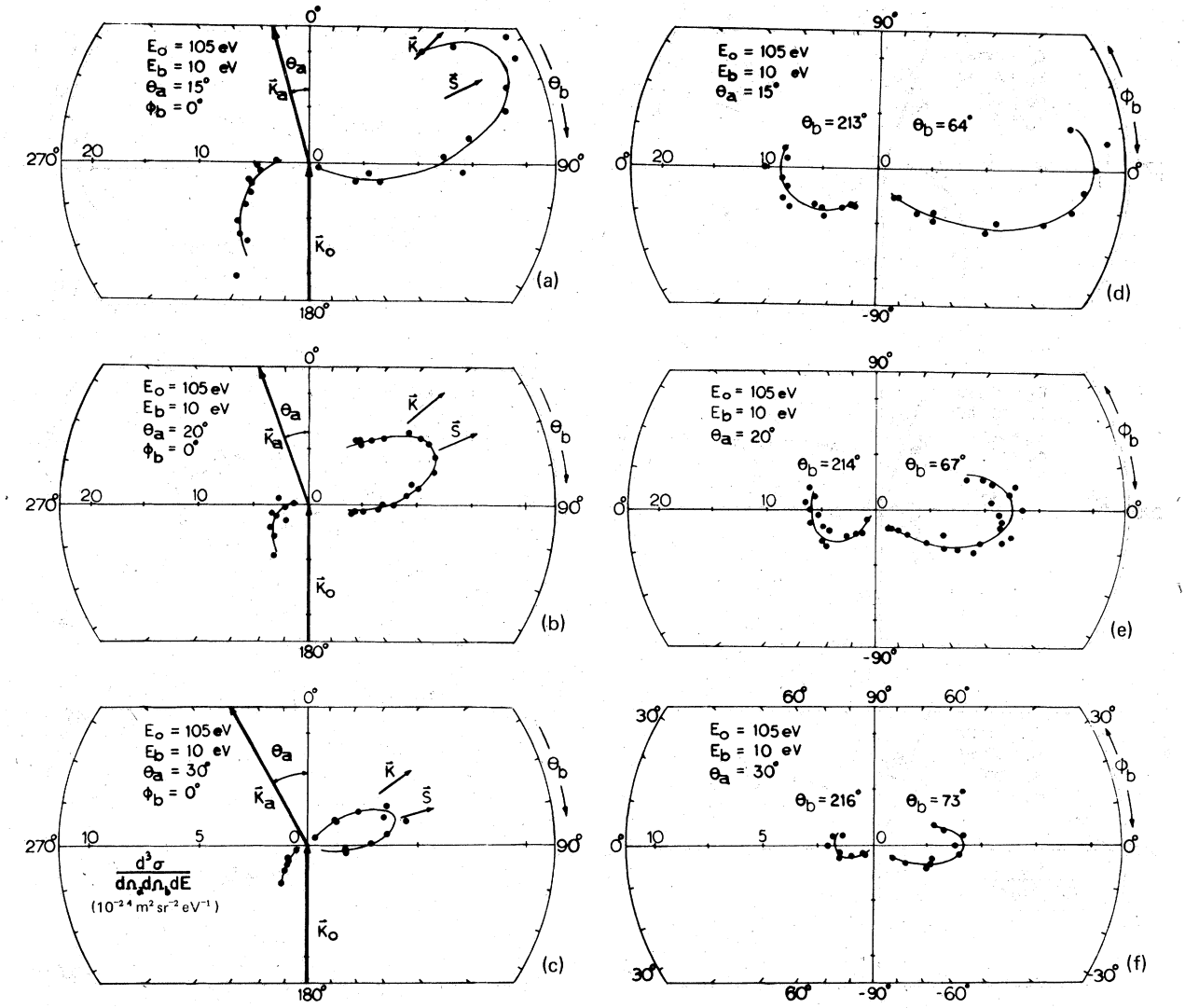

FIG. 2. Measurements for the case in which energy variables remained constants (E_0 = 105 eV, E_a = 70.42 eV, and E_b = 10 eV). The scattering angles are 15°, 20°, and 30° for (a)–(c), respectively. (a)–(c) are the results of the in-plane scans (ϕ_b = 0). Data shown on the right-hand side of (d)–(f) are the results of the vertical scans along the symmetric axes of their respective forward lobes. Data shown on the left-hand side of (d)–(f) are the vertical scans made as close to the maximum of the backward lobe as possible. The dots are the experimental data points. The curves are the lines fitting those data points to outline the shape of the triple-differential cross section.

and below the scattering plane agree with this symmetry.

Measurements presented in Fig. 2 are for the case in which energy variables remained constant (E_0 = 105 eV and E_b = 10 eV). Data were taken for the scattering angles θ_a = 15°, 20°, and 30°. As reported before[2,3,15] we observe two distinct lobes. The maximum magnitudes of the forward lobe increases as θ_a decreases. We established previously[15] that the triple-differential cross section is not cylindrically symmetric about the momentum-transfer direction as predicted by the Born approximation. One purpose of the current work is to see if the cross section is ever cylindrically symmetric about any axis. If so, we will call that axis the symmetry axis $\vec{S}$. By examining the results for the in-plane scans the forward lobes are approximately symmetric about certain axes. Therefore, we are able to choose an axis in the neighborhood of the ideal symmetry axis, and then scan a cone of half-angle 15° around that axis. Figure 4 shows the cone of half-angle θ_b' centered about a trial symmetry axis $\vec{S}$, which makes an angle ξ with the incident electron direction. ϕ_b' is the azimuthal angle

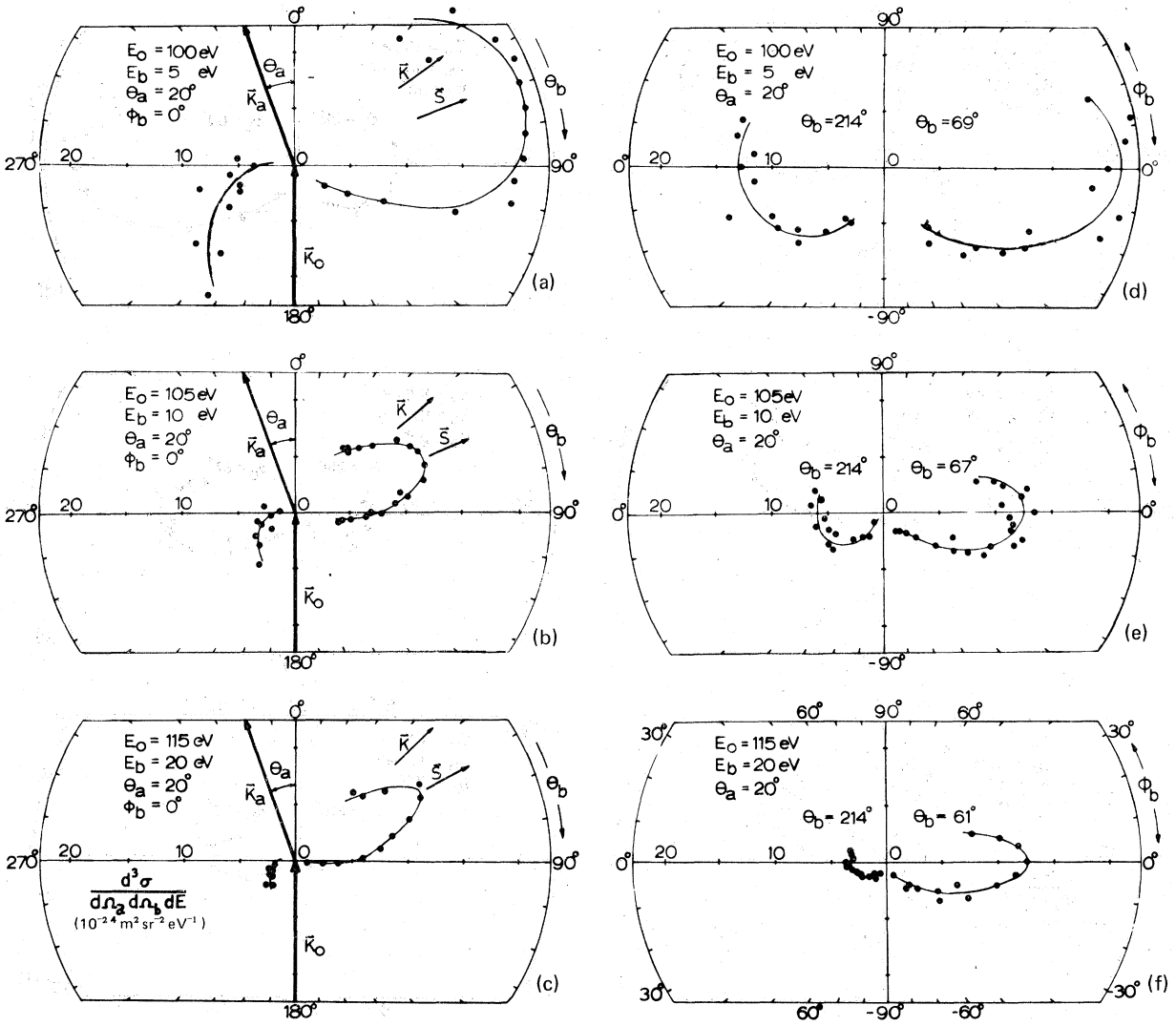

FIG. 3. Data presented as in Fig. 2 for the case in which the scattering angle was fixed at 20°. The ejected electron energies are 5, 10, and 20 eV for (a)–(c), respectively.

TABLE I. $E_0 = 105$ eV, $E_a = 70.42$ eV, and $E_b = 10$ eV.

θ_a	15°	20°	30°
Magnitude of the maximum of the forward peak (10^{-24} m^2 sr^{-2} eV^{-1})	20	12.4	4.2
Angle between the momentum transfer and the incident electron directions	45.4°	50.55°	54.62°
Angle between the symmetric axis and the incident electron direction	64°± 2°	67°± 2°	73°± 2°
Angle between the symmetric axis and the momentum-transfer direction	18.6°± 2	16.45°± 2	18.4°± 2
Angle subtended by the forward in-plane peak at its half maximum vertical	60°± 2° 60°± 2°	59°± 2° 60°± 2°	44°± 2° 48°± 2°
Angle subtended by the backward peak at its half maximum (vertical only)	102°± 2	104°± 2	70°± 2

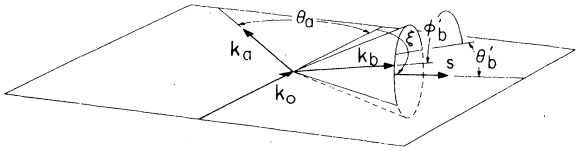

FIG. 4. Schematic diagram of the coordinates for a cone scan about an axis $\vec{S}$. The triple-differential cross section is measured as a function of the azimuthal angle ϕ_b'. $\vec{k}_0$, $\vec{k}_a$, and $\vec{k}_b$ are the directions of incoming and the two outgoing electrons, respectively. θ_b' is the half angle of the cone.

which locates the direction of the ejected electron along the surface of the cone. If the results of the scan turn out to be constant around the cone, the axis chosen will indeed be the symmetry axis. The results for a particular case of $E_0 = 105$ eV, $E_b = 10$ eV, and $\theta_a = 20°$ are presented in Fig. 5. Three half-angle 15° cone scans were made around the axis vectors in the plane at angles of 61°, 67°, and 73° with respect to the incident electron direction. The scan with $\xi = 67°$ produces a constant value, hence the axis along 67° with respect to the incident electron direction is the symmetry axis for this case. The determined symmetry axis is indicated by $\vec{S}$ in the diagram. For further evidence, we make a vertical scan along the determined symmetry axis. The results are shown in Figs. 2(d)–2(f). The shapes of the forward lobe in the plane and vertical scans are almost identical. The same procedures described above were performed for each different case. The forward lobes are cylindrically symmetric for all the cases shown here. For the present experimental arrangement, we could not reach the maximum of the backward lobe. Nevertheless we made vertical scans as close to the maximum as possible. The results are shown in Figs. 2(d)–2(f). θ_b is specified for each angular-

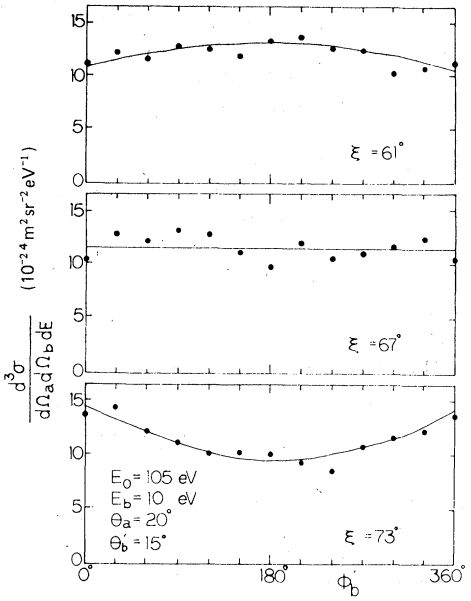

FIG. 5. Typical results of 15° half-angle cone scans. In this particular case, $E_0 = 150$ eV, $E_b = 10$ eV, and $\theta_a = 20°$. Three cone scans were made about the axes in the plane making angles of 61°, 67°, and 73° with the incident electron direction, respectively. Constant results of the cone scan show the axis along 67° with respect to the incident electron direction is the symmetric axis.

dependence plot. It is found that the backward lobe is much broader than the forward lobe. The facts observed from Fig. 2 are summarized in Table I.

Figure 3 shows another set of data for which the scattering angle was fixed at 20°. The energy of ejected electron E_b was varied from 5 to 10 to 20 eV. It is significant that the width of the lobes decreases as E_b increases. The forward lobes are

TABLE II. $E_a = 70.42$ eV and $\theta_a = 20°$.

E_0 (eV)	101	105	115
E_b (eV)	5	10	20
Magnitude of the maximum of the forward peak (10^{-24} m^2 sr^{-2} eV^{-1})	21	12.4	12.5
Angle between the momentum transfer and the incident electron direction	53.62°	50.55°	45.32°
Angle between the symmetric axis and the incident electron direction	69°±2	67°±2	61°±2
Angle between the symmetric axis and the momentum-transfer direction	15.38°±2	16.45°±2	16.8°±2
Angle subtended by the forward in-plane peak at its half maximum vertical	82°±2 82°±2	59°±2 60°±2	50°±2 52°±2
Angle subtended by the backward peak at its half maximum (vertical only)	112°±2	104°±2	90°±2

still found to be cylindrically symmetric. As shown in Fig. 2 the backward lobe is again broader than the forward lobe. The facts observed from Fig. 3 are summarized in Table II.

The angles between the momentum transfer and the incident electron directions vary significantly in both sets of data, as do the angles between the symmetry axes and the incident electron directions. It is interesting to note that the angles between the momentum-transfer vectors and the symmetry axes remain the same within the experimental error. This provides us a useful means to predict approximately the direction of the forward-lobe maximum.

VI. CONCLUSION

The triple-differential cross section of electron-impact ionization of helium consists of two distinct lobes. The forward lobe is found to be cylindrically symmetric. The backward lobe is broader than the forward lobe. It may also be cylindrically symmetric, but it does not share the same symmetry axis of the forward lobe.

ACKNOWLEDGMENT

We would like to thank G.H. Dunn for his comments on the manuscript.

---

*Staff member, Quantum Physics Division, National Bureau of Standards.

†Present address: Daimler-Benz A.G., Abt. Technische Physik, Stuttgart-Ut, West Germany.

‡On leave from the Dept. of Chemistry, Univ. of Maryland, College Park, Md. 20742.

[1]H. Ehrhardt, K. H. Hesselbacher, K. Jung, and K. Willmann, Case Stud. At. Phys. 2, 159 (1971).

[2]H. Ehrhardt, K. H. Hesselbacher, K. Jung, and K. Willmann, J. Phys. B 5, 1559 (1972).

[3]H. Ehrhardt, K. H. Hesselbacher, K. Jung, M. Schulz, and K. Willmann, J. Phys. B 5, 2107 (1972).

[4]H. Ehrhardt, K. H. Hesselbacher, K. Jung, E. Schubert, and K. Willmann, J. Phys. B 7, 69 (1974).

[5]K. Jung, F. Schubert, D. A. L. Paul, and H. Ehrhardt, J. Phys. B 8, 1330 (1975).

[6]K. Jung, E. Schubert, H. Ehrhardt, and D. A. L. Paul, J. Phys. B 9, 75 (1976).

[7]S. T. Hood, I. E. McCarthy, P. J. O. Teubner, and E. Weigold, Phys. Rev. A 8, 2494 (1973).

[8]S. T. Hood, E. Weigold, I. E. McCarthy, and P. J. O. Teubner, Nature 245, 65 (1973).

[9]S. T. Hood, I. E. McCarthy, P. J. O. Teubner, and E. Weigold, Phys. Rev. A 9, 260 (1974).

[10]E. Weigold, S. T. Hood, and I. E. McCarthy, Phys. Rev. A 11, 566 (1975).

[11]A. Ugbabe, E. Weigold, and I. E. McCarthy, Phys. Rev. A 11, 576 (1975).

[12]C. E. Brion, S. T. Hood, A. Hamnett, and J. Cook, in *The Tenth International Conference on the Physics of Electronic and Atomic Collisions: Abstracts of Papers*, (Commissariat á l'Energie Atomique, Paris, 1977), p. 380.

[13]R. Camilloni, A. Giardini-Guidoni, R. Tirribelli, and G. Stefani, Phys. Rev. Lett. 29, 618 (1972).

[14]M. A. Coplan, E. C. Brooks, III, and J. H. Moore, in Ref. 12, p. 378.

[15]E. C. Beaty, K. H. Hesselbacher, S. P. Hong, and J. H. Moore, J. Phys. B 10, 611 (1977).

[16]C. E. Kuyatt and J. A. Simpson, Rev. Sci. Instrum. 38, 103 (1967).

[17]M. V. Kurepa and L. Vuskovic, J. Phys. B 8, 2067 (1975).

[18]J. W. McConkey and J. A. Preston, J. Phys. B 8, 63 (1975).

[19]S. C. Gupta and J. A. Rees, J. Phys. B 8, 1267 (1975).

[20]R. H. J. Jansen, F. J. de Heer, H. J. Luyken, B. van Wingerden, and H. J. Blaauw, J. Phys. B 9, 185 (1976).